

# A hemispherical, high-solid-angle optical micro-cavity for cavity-QED studies

Guoqiang Cui, J. M. Hannigan, R. Loeckenhoff, F. M. Martinaga, M. G. Raymer

*Oregon Center for Optics and Department of Physics*

*University of Oregon, Eugene, OR 97403 USA \**

S. Bhongale, M. Holland

*JILA, University of Colorado, Boulder, CO 80309 USA<sup>†</sup>*

S. Mosor, S. Chatterjee, H. M. Gibbs, G. Khitrova

*Optical Science Center, University of Arizona, Tucson, AZ 85721 USA<sup>‡</sup>*

We report a novel hemispherical micro-cavity that is comprised of a planar integrated semiconductor distributed Bragg reflector (DBR) mirror, and an external, concave micro-mirror having a radius of curvature  $50\ \mu\text{m}$ . The integrated DBR mirror containing quantum dots (QD), is designed to locate the QDs at an antinode of the field in order to maximize the interaction between the QD and cavity. The concave micro-mirror, with high-reflectivity over a large solid-angle, creates a diffraction-limited (sub-micron) mode-waist at the planar mirror, leading to a large coupling constant between the cavity mode and QD. The half-monolithic design gives more spatial and spectral tuning abilities, relatively to fully monolithic structures. This unique micro-cavity design will potentially enable us to both reach the cavity quantum electrodynamics (QED) strong coupling regime and realize the deterministic generation of single photons on demand.

## I. INTRODUCTION

Optical micro-cavities have played a central role in achieving strong coupling between a single atom and a mode of an optical cavity, which enables a range of novel phenomena that rely on the control of the mode structure of the vacuum (so-called cavity-QED effects). These include enhanced or suppressed spontaneous emission [1, 2, 3, 4, 5, 6], thresholdless lasing [7, 8], normal-mode splitting [9], and optical nonlinearity at the single-photon level [10]. In the last two decades, such strong coupling has been achieved in free-space atomic systems, such as a dilute atomic beam passing through a short ( $10\text{--}100\ \mu\text{m}$  length) optical cavity [11, 12, 13], or through a cold microwave

---

\*Electronic address: raymer@uoregon.edu

<sup>†</sup>Electronic address: mholland@bdagger.colorado.edu

<sup>‡</sup>Electronic address: hyattgibbs@att.net

cavity [14].

There is also interest in achieving strong cavity-QED coupling in semiconductor QD systems, following early studies using planar quantum-well-cavity systems, which themselves cannot reach this regime [15]. Recent experiments showed signatures of strong coupling in some monolithic structures such as micro-pillar [16], photonic crystal nanocavity [17] and micro-disk [18]. Obvious advantages of using QDs in such schemes are that the QDs are stationary and they exist in a solid-state system, which can be optically or electrically pumped [19]. The principal disadvantages in these monolithic structures, however, are the lack of efficient control of the spatial and spectral overlap between QDs resonance and cavity modes. For instance, temperature tuning of the QD has to be used to tune through cavity resonance [16, 17, 18], which is undesirable because the dipole dephasing rate increases at elevated temperatures [20, 21].

This report focuses on the design, modeling, fabrication, and performance of a unique half-monolithic, hemispherical micro-cavity for semiconductor cavity-QED. The cavity parameters are in a novel range: cavity length = 40 – 60  $\mu\text{m}$ , finesse = 200 (which should be amenable to increase by an order of magnitude), mode-waist size  $\approx 1 \mu\text{m}$ , mode divergence angle  $\pm 40$  deg. This cavity design contains two unique features—the use of a concave micro-mirror with high-reflectivity over a large-solid angle and the use of an integrated DBR mirror containing the QD sample in an external-cavity configuration. The 40–60-micron curved mirror substrate has a high degree of sphericity and an excellent surface quality, enabling the application of a custom-designed multilayer dielectric coating with 99.5% reflectivity over a high-solid-angle [22]. Such large solid angle is unique compared with, for example, a recently reported half-monolithic micro-cavity design [23].

One potential application of such a cavity/QD system is for semiconductor cavity-QED study; the other is the generation, on demand, of single photons or of photon pairs. The cavity can also be operated with a standard planar dielectric mirror replacing the semiconductor DBR mirror. Such an all-dielectric cavity may find uses in atomic cavity-QED or cold-atom studies, or in novel forms of microscopy or interferometry.

The cavity components have been fabricated in our collective laboratories—the concave micro-mirror by a novel gas-bubble technique and the DBR/QD structure by molecular-beam epitaxy (MBE).

## II. CAVITY DESIGN OVERVIEW

Figure 1 shows a real structure and a schematic diagram of the cavity. A transparent, planar substrate with a multilayer DBR coating (made either of semiconductors or optical coating dielectrics) forms one end of the cavity. A transparent concave glass surface with a dielectric multilayer reflective coating forms the other end. In between is air or vacuum. The radius of curvature of the mirror is denoted  $R_M$ , and can be fabricated in the range  $40 - 100 \mu\text{m}$ . The on-axis distance  $L$  between the surfaces of the two mirrors is referred to as the cavity length. In a hemispherical cavity these lengths are equal,  $L = R_M$ . This places the cavity on the boundary for stability, and (in the paraxial approximation, which actually fails here) leads to the interesting property that the modes fall into groups with a high degree of frequency degeneracy [24].

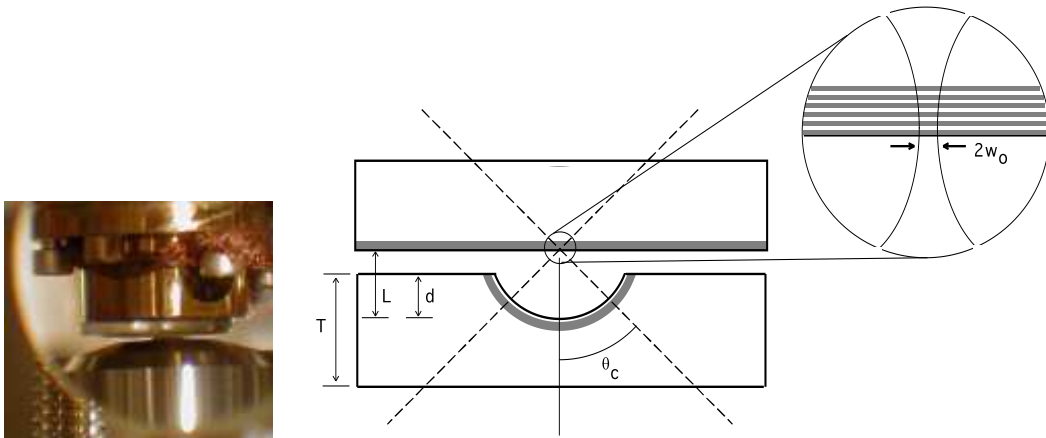


FIG. 1: Hemispherical cavity, comprised of a planar substrate and a concave glass surface with layer reflective coating (shown as grey region). The dashed lines approximate the  $1/e$  intensity contours of the fundamental mode in the cavity and its continuation outside. The angular half-width of the mode is  $\theta_C$ . The blow-up shows the DBR and the mode contours in the waist region. Typically the length  $L$  is  $50 \mu\text{m}$ , the depth  $d$  is  $30 \mu\text{m}$  and the waist diameter is  $2w_0 = 1 \mu\text{m}$ .

The radius of the mode waist, located at the planar mirror, is denoted  $w_0$ . Since the QD is to be placed in this waist, this radius should be minimized in order to maximize the coupling between the QD and the field. The angular half-width of the cavity mode is  $\theta_C$ . Diffraction dictates that the smaller  $w_0$  is made, the larger  $\theta_C$  becomes. When  $w_0$  equals one optical wavelength, the angle  $\theta_C$  is roughly  $40 \text{ deg}$ . For such large angles, the electromagnetic field cannot be completely transverse to the cavity axis, as would be the case in the paraxial limit where  $\theta_C$  is restricted to very small values. This indicates a need for a theory, summarized below, beyond the common paraxial treatment.

The effective mode volume  $V_{\text{eff}}$ , which depends on the location of the QD, is defined as spatial integral of the field intensity, normalized to unity at the maximum. For example, if the mode amplitude can be described as a (paraxial) Gaussian function with  $1/e$  amplitude contours that define a spot size  $w(z)$  at the position  $z$  along the cavity axis, then the effective mode volume is given by  $V_{\text{eff}} = \pi w_0^2 L/4$  [25]. It is thus important to locate the QD at an antinode of the field at the waist.

### A. Concave Micro-mirror Substrate

A unique component of our cavity is the concave micro-mirror. We developed a technique for its in-house fabrication. For use in a high-finesse cavity, it is crucial that the curved surface of the mirror substrate be smooth on nanometer scales. This prevents undue amounts of light scattering that would act as a loss, spoiling the finesse.

Our technique, shown in Fig. 2(a), proceeds by melting a stack of small, high-quality borosilicate glass tubes under a nitrogen atmosphere, trapping small gas bubbles. By surface tension the gas bubbles are naturally created with high degree of sphericity. After the glass cools and hardens, we grind and polish it on a simple optical polishing wheel so that about one-third of a selected bubble remains embedded in the surface. The top surface, where a few bubbles are open, is finished with diamond disc featuring nickel-plated diamonds in a raised dot matrix pattern of  $6\ \mu\text{m}$  grit size on a polishing wheel. The bottom surface is polished using a  $0.05\ \mu\text{m}$  colloidal silica suspension on a polishing cloth, to achieve an optical-quality finish. Finally, we obtain a flat sample of about  $T = 150\ \mu\text{m}$  thickness, which forms our concave mirror substrate.

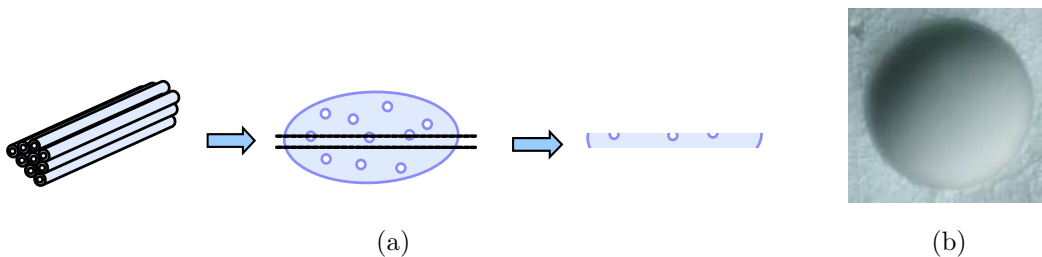


FIG. 2: (a) Melting borosilicate glass tubes to form nitrogen gas-bubbles in the glass and polishing the glass bulk into a  $150\ \mu\text{m}$ -thick slide. (b) 40X pictures of a dimple. Diameter of the dimple =  $200\ \mu\text{m}$ .

Figure 2(b) shows images of a typical dimple at 40X magnification. The planar surface on the top side, surrounding the dimples, is very rough, as a result of the final  $6\ \mu\text{m}$ -grit used on this side. This was chosen to minimize the amount of contaminating sub-micron glass dust produced during

polishing. The inside of the dimple (out of focus here) is far smoother. The dimples will ideally have an opening half-angle of  $\theta_C \approx 40$  deg, a radius of curvature of  $R_M \approx 50 \mu\text{m}$  and a surface with sub-nm roughness.

We expected a good sphericity of the dimple surfaces since for decreasing dimensions the surface tension is an increasingly strong force compared to other forces like gravity. The sphericity has been measured with a Wyko interferometer, see Fig. 3. At the bottom of a dimple, in a circle of  $15 \mu\text{m}$  diameter, the deviations from perfect sphericity were found to be less than 10 nm.

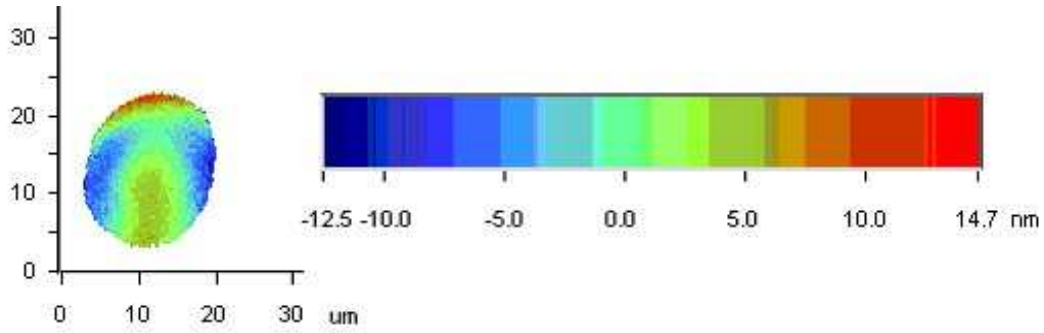


FIG. 3: Measured sphericity of the dimple with a Wyko interferometer at the University of Arizona.

The surface roughness was also measured using a Wyko interferometer that carries out a Fourier-analysis of the surface to determine the power (spatial) spectral density (PSD) of surface roughness as a function of the lateral size of the errors. Figure 4(a) shows the measured PSD of five dimples.

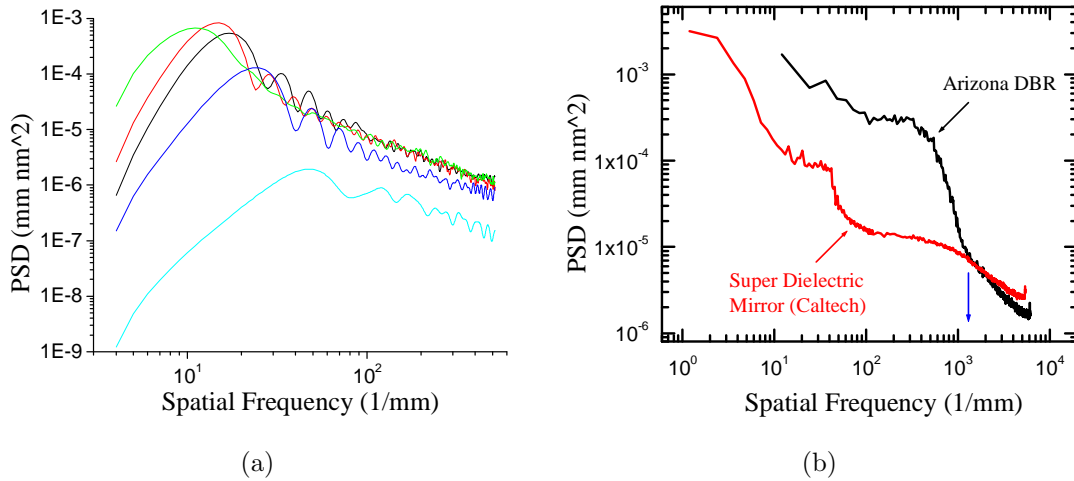


FIG. 4: (a) Measured PSD surface roughness for five dimples and (b) semiconductor DBR mirror and super dielectric mirror with a Wyko interferometer. The relevant length scale (indicated by the blue arrow) is about one micron because our unique cavity design yields a waist size at the DBR of this size.

For errors with a transverse spatial frequency greater than  $300 \text{ mm}^{-1}$ , the surface quality com-

petes with the best planar mirrors available, see Fig. 4(b). However the roughness increases dramatically for smaller spatial frequencies (large length scales). We are not sure whether this represents intrinsic errors like wrinkles formed in the cooling process or debris left from polishing.

### B. Optical Coating for Curved Micro-Mirror

Optical coating of such a small and highly curved dimple substrate is a nonstandard procedure. One problem is that the atomic coating beam is incident on the curved substrate at a different angle at each different location. This alters the deposition rate in a location-dependent manner, which leads to systematic variation of the layer thickness and therefore of edge wavelengths of the coating's stop-band. Therefore, we designed the coating scheme (using TFCalc), in a way that compensates for the large change of coating-beam angle across the surface of the substrate.

We designed a high-index-contrast TiO<sub>2</sub>-SiO<sub>2</sub> coating, having a stop-band shifted to longer wavelength at the center of the dimple. For a working wavelength of 750 nm, the reflectivity is greater than 95% between 737 nm and 808 nm. For locations away from the center, the coating becomes thinner, shifting the stop band to shorter wavelengths. At some location on the dimple surface (or angle from the optical axis at the mode focus region), the stop band suddenly shifts past the working wavelength, causing a sudden drop of mirror reflectivity, as has also been observed in [23].

Measurements, shown in Fig. 5(a), of the dimple-mirror transmission versus angle from the optical axis confirms that our design and fabrication has succeeded in giving a high reflectivity (99.5% or higher) over a wide angular range of  $\pm 40$  deg, which is wide enough to support the hemispherical modes of interest. The coated curved dimple was then glued, using index-matching optical adhesive, to the face of a 100X immersion-microscope objective (Zeiss Plan-NEOFLUAR) with a numerical aperture  $NA = 1.3$  in order for efficient mode-coupling over a high-solid angle, see Fig. 5(b). To ensure proper positioning of the dimple, we glue it while monitoring interferometrically by a Twyman-Green setup [26], in which a laser beam passes into the objective, reflects from the dimple and interferences with a reference beam.

### C. MBE-Growth and Characterization of Integrated Top Mirror and QD layer

Semiconductor planar DBR mirror with exceptionally good surface smoothness and high reflectivity can be grown by MBE technique [27], We found that the surface roughness on transverse

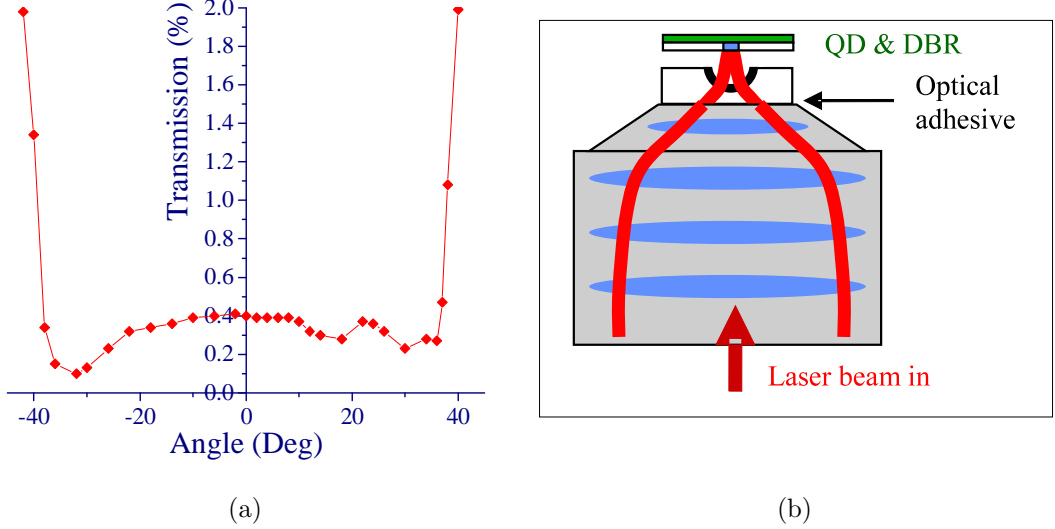


FIG. 5: (a) Measured dimple-mirror transmission versus angle from the optical axis at the mode focus region. (b) The coated curved dimple is glued using index-matching optical adhesive to the face of a 100X immersion-microscope objective with  $NA=1.3$ .

length scales relevant for our needs ( $\sim 1$  micron) is equal to that of the best super-polished dielectric mirrors of the type used in atomic cavity-QED experiments.

Figure 4(b) shows a comparison of two kinds of mirrors—the MBE-grown and a commercial super polished dielectric mirror (made by Kimble group at the Caltech). The figure plots the PSD of surface roughness versus transverse spatial frequency, measured with a Wyko interferometer. It is seen that the planar semiconductor mirror has far larger roughness for low spatial frequencies, while the commercial dielectric mirror is slightly rougher at spatial frequencies above  $100 \text{ mm}^{-1}$ , the region of interest for our cavity, since the mode waist is less than  $1 \mu\text{m}$ .

The GaAs QDs that we use are interface-fluctuation quantum dots (IFQDs). They are formed through the influence of monolayer-thick interface fluctuation during the MBE-growth of a quantum well (QW), creating elliptically shaped regions about 50–100 nm across [28, 29]. We have succeeded in growing good-quality IFQDs on the top surface of high-quality DBRs. The QDs are embedded in a wavelength-thick spacer layer to place the QDs at an antinode of the cavity and have a relatively large dipole moment (60 Debye), enabling them to interact strongly with the cavity field.

Figure 6 shows a set of nano-scope photoluminescence (PL) spectra [29] for a sequence of different locations with a spatial step of 300 nm in the QW plane on such a DBR. The broader PL emission lines in the upper traces are inhomogeneously broadened and can be fit approximately by Gaussian distributions, and are likely caused by emission from spatially close QDs with different lateral sizes and hence different emission frequencies. Some of the narrower PL emission lines in the

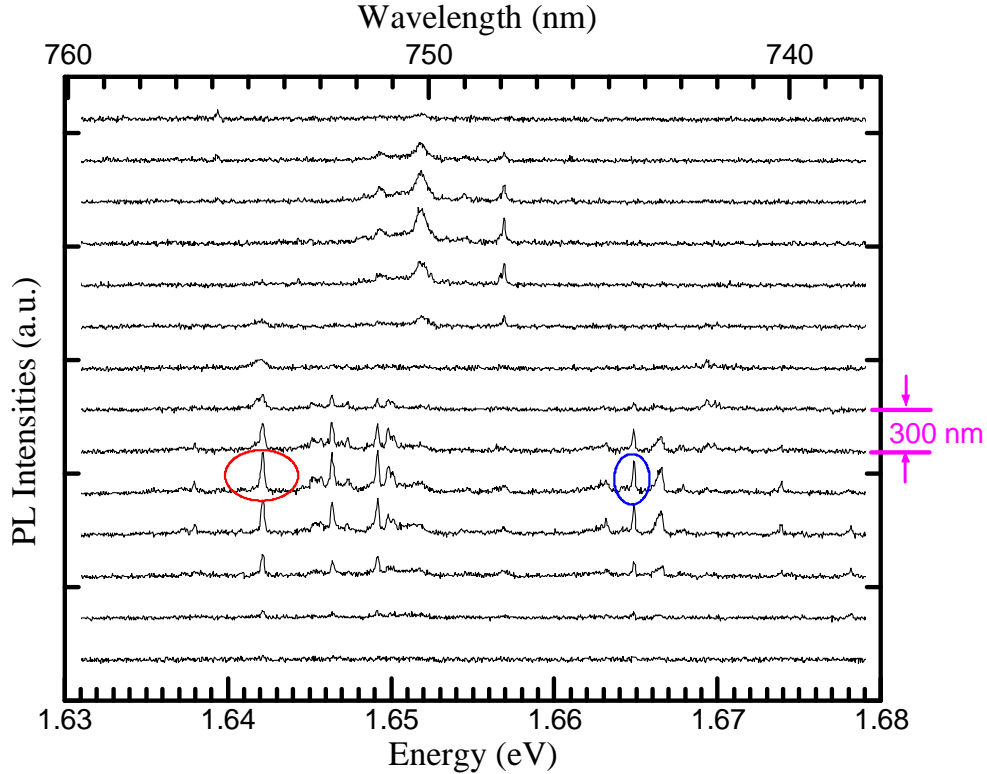


FIG. 6: Nano-scope spectral scans of different spatial locations on UA-grown sample, showing both spectrally and spatially well isolated single QD emission line (red circled) at low temperature in the 750–760 nm target region.

lower traces can be fit by Lorentzian distributions, which are homogeneously broadened, signifying isolated single quantum emitters, and can be identified as emissions from single QDs, for example, the red circled and blue circled ones. The red circled one is in our 750–760 nm target region and is spectrally well isolated. The emission lines at the same energy (wavelength) in the adjacent traces are also from this specific QD and indicate that it is also spatially well isolated ( $\sim 600$  nm) from other QDs.

### III. CAVITY CONSTRUCTION, TESTING AND MODELING

We constructed and tested a high-quality hemispherical cavity using our 60-micron mirror and a planar semiconductor DBR (CAT 96) containing QDs located at the center of a one-wavelength spacer layer. The semiconductor DBR mirror is mounted on a tripod system, supported by three Burleigh UHVL Inchworm Motors, to control precisely its longitudinal position and its angle with respect to the curved mirror. The tripod also contains an  $x$ - $y$  nano-positioner, which can laterally



scan the mode waist in a  $50 \times 50 \mu\text{m}^2$  region, essential for scanning and addressing a single QD, and a piezoelectric stack driven by a laser-referenced feedback loop for stabilizing the length of the cavity. The system operates inside a high-vacuum chamber ( $10^{-8}$  torr), to allow cooling the DBR mirror to around 10–17 K to reduce QD dephasing rates and to avoid coating of the DBR mirror by cryopumping and attendant absorption and scattering.

### A. Cavity-mode structure and finesse

We tested the cavity by passing laser light through it and observing the cavity modes and measuring its finesse. Figure 7 shows several well-defined cavity modes observed for different frequencies. We label them using HG and LG notation, since they are qualitatively similar to the Hermite-Gauss or Laguerre-Gauss modes that are applicable in the paraxial limit [24].

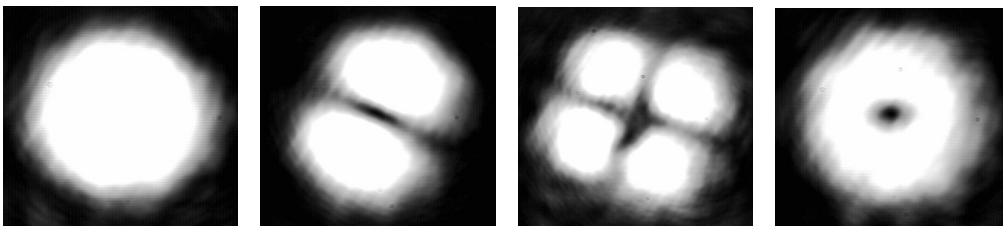


FIG. 7: Measured images of modes of  $60 \mu\text{m}$  micro-cavity. The modes are HG00, HG01, HG11 and LG01, from left to right, respectively.

We measured the transmission versus laser wavelength for a cavity containing a layer of QDs. The transverse-mode frequency-spacings become smaller as we approach the hemispherical limit by making the cavity longer. Our results are consistent with predictions for the hemispherical limit, paraxial-mode theory [24], which predicts degenerate sets of modes, separated by  $c/4L$ , where  $L$  is the cavity length.

Figure 8 shows two scans over the range of wavelength where the QDs absorb (750–760 nm). The finesse is about 50 at room temperature. When we do a similar scan near 780 nm, where there is less absorption, the finesse increases to 200. This is an indication that we are observing cavity-enhanced absorption by the QD layer. The predicted finesse is 600 based on reflectivity measurements of the mirror alone. The lowered finesse is likely due to residual contamination in the mirror dimple.

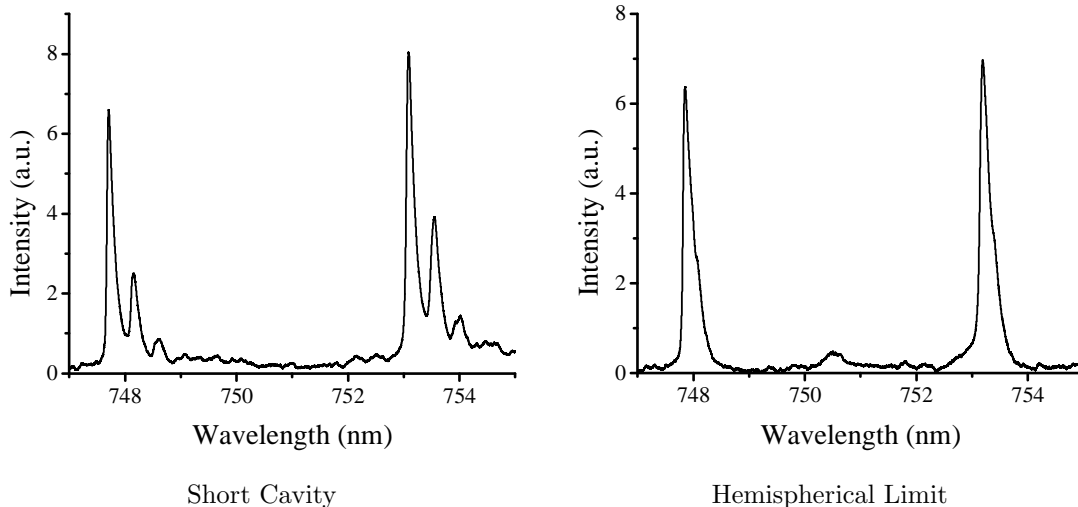


FIG. 8:  $60\ \mu\text{m}$  cavity transmission spectra with QDs at antinode. The cavity finesse is about 50 at room temperature.

### B. Modeling the micro-cavity modes

The QD-mode coupling strength is proportional to the amplitude of the normalized cavity mode at the location of the QD. In order to make the coupling very strong, it is necessary to localize highly the transverse extent of the mode function in the vicinity of the QD, and align the mode polarization vector with the dipole transition matrix element of the QD. Determining the precise degree to which this localization is possible is nontrivial, since the mode structure for such a small cavity is non-paraxial, is non-separable into polarization components, and is non-separable into longitudinal and transverse modes [30].

We have taken two approaches to modeling the modes of the near-hemispherical micro-cavity. The two approaches are a fully numerical one—finite-difference-time-domain (FDTD) [31], and a hybrid analytic-numerical method [32]. The computations account fully for the distributed nature of the planar DBR mirror, an important aspect since plane waves of different incident angles undergo different phase shifts upon reflection there. The curved mirror is treated as a perfect reflector, an approximation expected to be adequate since the mode wave fronts are well matched to the mirror curvature. An example of the FDTD method, showing the calculated energy density of the mode versus position, is shown in Fig. 9. The calculations show that even in the presence of the DBR angle-dependent phase shifts, the mode waist in the non-paraxial regime is smaller than one wavelength.

An interesting result of the hybrid analytic-numerical method is a novel DBR-induced spin-orbit

coupling of modes, which leads to small frequency splitting previously not identified [32]. The method also predicts a spatial splitting of the fundamental Gaussian mode (and other Gaussian modes) into a non-axis-symmetric inverted “V” shape.

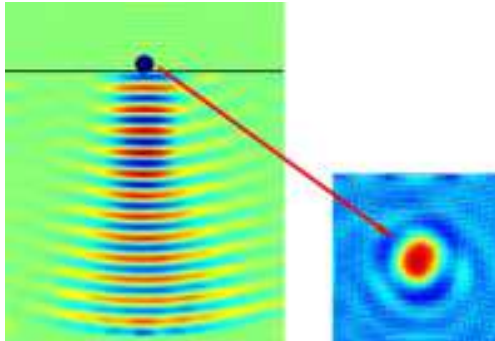


FIG. 9: Numerical model for micro-cavity mode energy density, where the planar DBR structure is at the top and the curved mirror is in the lower half of the figure. The QD sits in a bright local maximum region in the first layer of the DBR. The results indicate that the mode waist is of the order of one wavelength.

#### IV. APPLICATION

The hemispherical micro-cavity we have fabricated has an excellent prospect to achieve both strong coupling and efficient generation of single- and pair-photons on demand. The hemispherical design is geometrically stable with the only loss (other than surface scatter) being by transmission through the end mirrors, not by diffraction losses as occurs in other micro-structures [33]. The use of a concave micro-mirror with high-reflectivity over a high-solid-angle makes the mode waist size at the planar DBR diffraction limited and consequently leads to a large coupling strength. It enables a direct out-coupling of the spontaneously emitted single photons into a single-mode traveling wave, which is highly desirable for the efficient and on-demand single-photon generation. In addition, our system uses a cavity with adjustable length and a transversely movable focal region, allowing good spatial and spectral overlap of QD resonances with high-Q cavity modes.

##### A. Cavity QED Strong Coupling

Cavity-QED strong coupling occurs when the electric-dipole interaction frequency between an atom or QD and a single, unoccupied mode exceeds the energy decay rates of the composite system. The signature of strong coupling is a frequency splitting in the laser transmission spectrum approximately equal to the twice of the coupling constant, so called the normal-mode-splitting,

which arises from the coherent interaction of two degenerate systems—the single QD and the single cavity mode. Such splitting can be viewed as a lifting of degeneracy.

IFQDs can have dipole moments as large as 60–100 Debye [34], yielding a vacuum Rabi splitting of 49 – 81  $\mu\text{eV}$ , assuming a cavity waist of 1 micron and a cavity length of 50 microns. As required for strong coupling, this projected splitting would exceed the sum of the oscillator dissipation linewidth, typically 15  $\mu\text{eV}$ , and the cavity dissipation linewidth, 8  $\mu\text{eV}$  for a length of 50 microns and a reflectivity of 0.996.

The transmission of an empty Fabry-Perot cavity has a series of single peaks with high transmission at each resonance. In the strong-coupling regime one of the peaks splits into two peaks, the one in resonance with the QD transition, with a minimum located at the position of former peak. This shows a strong enhancement of system absorption at resonance. This interaction is suitable for coherent quantum engineering concepts such as those being developed in attempts to achieve quantum-information processing [35, 36].

## B. Photons on Demand

Another important application of such strongly coupled cavity-QD systems is the deterministic generation of single photons [37, 38, 39] or of photon pairs on demand [40]. Such sources have wide applications in the emerging field of quantum information science [41]. This is particularly true for quantum cryptography, in which an essential element of secure quantum key distribution (QKD) is an optical source emitting a train of pulses that contain one and only one photon [42]. For example, a source having zero probability for generating two or more photons in a pulse and greater than 20% probability of generating one photon would lead to a great advance in QKD in daylight through the atmosphere [43, 44, 45].

The high quality of the concave mirror substrate in our design opens the possibility for very high cavity finesse. Currently we are working to design a 99.95% reflectivity coating, which should achieve a finesse approaching 6,300. The unknown in this is how smooth and regular the coating can be, when applied using standard beam coating in such a small dimple. MBE-growth technique will enable one to grow two QWs with a several-nanometer separation, with a large enough barrier potential to prevent electron tunneling, where IFQDs formed in each QW are each doped with an excess electron. Quantum information processing can be implemented using this structure for qubit storage and gate operation [46], while cavity modes used for transferring quantum information between pairs of QDs. The cavity design should also lend itself to applications in atomic quantum

optics [47] as well as semiconductor optics [48].

### Acknowledgments

This work was supported by the National Science Foundation grant no. ECS-0323141 and by the Army Research Office grant no. DAAD19-99-1-0344.

- 
- [1] E. M. Purcell, "Spontaneous emission probabilities at radio frequencies (Abstract)," *Phys. Rev.* **69**, 681 (1946).
  - [2] R. G. Hulet, E. S. Hilfer, and D. Kleppner, "Inhibited spontaneous emission by a Rydberg atom," *Phys. Rev. Lett.* **55**, 2137 (1985).
  - [3] F. De Martini, G. Innocenti, G. R. Jacobovitz, and P. Mataloni, "Anomalous spontaneous emission time in a microscopic optical cavity," *Phys. Rev. Lett.* **59**, 2955 (1987).
  - [4] D. J. Heinzen, J. J. Childs, J. E. Thomas, and M. S. Feld, "Enhanced and inhibited visible spontaneous emission by atoms in a confocal resonator," *Phys. Rev. Lett.* **58**, 1320 (1987).
  - [5] D. J. Heinzen and M. S. Feld, "Vacuum radiative level shift and spontaneous-emission linewidth of an atom in an optical resonator," *Phys. Rev. Lett.* **59**, 2623 (1987).
  - [6] S. E. Morin, C. C. Yu, and T. W. Mossberg, "Strong atom-cavity coupling over large volumes and the observation of subnatural intracavity atomic linewidths," *Phys. Rev. Lett.* **73**, 1489 (1994).
  - [7] Y. Yamamoto and R. E. Slusher, "Optical processes in microcavities," *Phys. Today* **46**, 66 (1993).
  - [8] P. R. Rice and H. J. Carmichael, "Photon statistics of a cavity-QED laser: a comment on the laser-phase-transition analogy," *Phys. Rev. A* **50**, 4318 (1994).
  - [9] H. J. Kimble, "Structure and dynamics in cavity quantum electrodynamics," in *Cavity Quantum Electrodynamics*, P. Berman ed. (Academic Press, San Diego, 1994), pp. 203-266.
  - [10] Q. A. Turchette, C. J. Hood, W. Lange, H. Mabuchi, and H. J. Kimble, "Measurement of conditional phase shifts for quantum logic," *Phys. Rev. Lett.* **75**, 4710 (1995).
  - [11] D. Meschede, H. Walther, and G. Müller, "One-atom maser," *Phys. Rev. Lett.* **54**, 551 (1985).
  - [12] M. Brune, J. M. Raimond, P. Goy, L. Davidovich, and S. Haroche, "Realization of a two-photon maser oscillator," *Phys. Rev. Lett.* **59**, 1899 (1987).
  - [13] G. Rempe, R. J. Thompson, R. J. Brecha, W. D. Lee, and H. J. Kimble, "Optical bistability and photon statistics in cavity quantum electrodynamics," *Phys. Rev. Lett.* **67**, 1727 (1991).
  - [14] S. Haroche and D. Kleppner, "Cavity quantum electrodynamics," *Physics Today* **42**, 24 (1989).
  - [15] G. Khitrova, H. M. Gibbs, F. Jahnke, M. Kira, and S. W. Koch, "Nonlinear optics of normal-mode-coupling semiconductor microcavities," *Rev. Mod. Phys.* **71**, 1591 (1999).
  - [16] J. P. Reithmaier, G. Sek, A. Löffler, C. Hofmann, S. Kuhn, S. Reitzenstein, L. V. Keldysh, V. D.

- Kulakovskii, T. L. Reinecke, and A. Forchel, “Strong coupling in a single quantum dot-semiconductor microcavity system,” *Nature* **432**, 197 (2004).
- [17] T. Yoshie, A. Scherer, J. Hendrickson, G. Khitrova, H. M. Gibbs, G. Rupper, C. Ell, O. B. Shchekin, and D. G. Deppe, “Vacuum Rabi splitting with a single quantum dot in a photonic crystal nanocavity,” *Nature* **432**, 200 (2004).
- [18] E. Peter, P. Senellart, D. Martrou, A. Lemaitre, J. Hours, J. M. Gérard, and J. Bloch, “Exciton-photon strong-coupling regime for a single quantum dot embedded in a microcavity,” *Phys. Rev. Lett.* **95**, 067401 (2005).
- [19] Z. Yuan, B. E. Kardynal, R. M. Stevenson, A. J. Shields, C. J. Lobo, K. Cooper, N. S. Beattie, D. A. Ritchie, and M. Pepper, “Electrically driven single-photon source,” *Science* **295**, 102 (2002).
- [20] X. Fan, T. Takagahara, J. E. Cunningham, and H. Wang, “Pure dephasing induced by exciton-phonon interactions in narrow GaAs quantum wells,” *Solid State Commun.* **108**, 857 (1998).
- [21] M. Bayer and A. Forchel, “Temperature dependence of the exciton homogeneous linewidth in  $\text{In}_{0.6}\text{Ga}_{0.4}\text{As}/\text{GaAs}$  self-assembled quantum dots,” *Phys. Rev. B* **65**, 041308(R) (2002).
- [22] The coating was made by *Spectrum Thin Films Company*, New York.
- [23] M. Trupke, E. A. Hinds, S. Eriksson, and E. A. Curtis, “Microfabricated high-finesse optical cavity with open access and small volume,” arXiv:quant-ph/**0506234** (2005).
- [24] A. E. Siegman, in *Lasers*, (University Science Books, Mill Valley, CA, 1986).
- [25] P. D. Drummond, “Optical bistability in a radially varying mode,” *IEEE J. Quantum Electron.* QE-**17**, 301 (1981).
- [26] M. Born and E. Wolf, in *Principles of Optics* (7th Ed.), (Cambridge University Press, New York, 1999) pp. 338-340.
- [27] R. P. Stanley, R. Houdré, U. Oesterle, M. Gailhanou, and M. Ilegems, “Ultrahigh finesse microcavity with distributed Bragg reflectors,” *Appl. Phys. Lett.* **65**, 1883 (1994).
- [28] A. Zrenner, L. V. Butov, M. Hagn, G. Abstreiter, G. Bohm, and G. Weimann, “Quantum dots formed by interface fluctuations in AlAs/GaAs coupled quantum well structures,” *Phys. Rev. Lett.* **72**, 3382 (1994).
- [29] D. Gammon, E. S. Snow, B. V. Shanabrook, D. S. Katzer, and D. Park, “Fine structure splitting in the optical spectra of single GaAs quantum dots,” *Phys. Rev. Lett.* **76**, 3005 (1996).
- [30] D. H. Foster and J. U. Nöckel, “Methods for 3-d vector microcavity problems involving a planar dielectric mirror,” *Opt. Commun.* **234**, 351 (2004).
- [31] M. Pelton, J. Vuckovic, G. S. Solomon, A. Scherer, and Y. Yamamoto, “Three-dimensionally confined modes in micropost microcavities: quality factors and Purcell factors,” *IEEE J. Quantum Electron.* **38**, 170 (2002).
- [32] S. Bhongale, M. Holland, and M. G. Raymer, “Quantum dot quantum computing: non-paraxial eigenmodes of microcavity,” presented at the APS 34th Meeting of the Division of AMO Physics, Boulder, CO, 20-24 May 2003.

- [33] J. Vuckovic, M. Pelton, A. Scherer, and Y. Yamamoto, “Optimization of three-dimensional micropost microcavities for cavity quantum electrodynamics,” *Phys. Rev. A* **66**, 023808 (2002).
- [34] L. C. Andreani, G. Panzarini, and J. M. Gérard, “Strong-coupling regime for quantum boxes in pillar microcavities: theory,” *Phys. Rev. B* **60**, 13276 (1999).
- [35] T. Pellizzari, S. Gardiner, J. Cirac, and P. Zoller, “Decoherence, continuous observation, and quantum computing: a cavity QED model,” *Phys. Rev. Lett.* **75**, 3788 (1995).
- [36] J. I. Cirac, P. Zoller, H. J. Kimble, and H. Mabuchi, “Quantum state transfer and entanglement distribution among distant nodes in a quantum network,” *Phys. Rev. Lett.* **78**, 3221 (1997).
- [37] A. Kuhn, M. Hennrich, and G. Rempe, “Deterministic single-photon source for distributed quantum networking,” *Phys. Rev. Lett.* **89**, 067901 (2002).
- [38] A. Kiraz, C. Reese, B. Gayral, L. Zhang, W. V. Schoenfeld, B. D. Gerardot, P. M. Petroff, E. L. Hu, and A. Imamoglu, “Cavity-quantum electrodynamics with quantum dots,” *J. Opt. B: Quantum Semiclass. Opt.* **5**, 129 (2003).
- [39] J. McKeever, A. Boca, A. D. Boozer, R. Miller, J. R. Buck, A. Kuzmich, and H. J. Kimble, “Deterministic generation of single photons from one atom trapped in a cavity,” *Science* **303**, 1992 (2004).
- [40] T. M. Stace, G. J. Milburn, and C. H. W. Barnes, “Entangled two-photon source using biexciton emission of an asymmetric quantum dot in a cavity,” *Phys. Rev. B* **67**, 085317 (2003).
- [41] D. Bouwmeester, A. Ekert, and A. Zeilinger, in *The Physics of Quantum Information* (Springer, Berlin, 2000).
- [42] C. H. Bennett, G. Brassard, and A. Ekert, “Quantum cryptography,” *Sci. Am.* **267**, 50 (1992).
- [43] R. J. Hughes, J. E. Nordholt, D. Derkacs, and C. G. Peterson, “Practical free-space quantum key distribution over 10 km in daylight and at night,” *New J. Phys.* **4**, (2002).
- [44] K. J. Resch, M. Lindenthal, B. Blauensteiner, H. R. Böhm, A. Fedrizzi, C. Kurtsiefer, A. Poppe, T. Schmitt-Manderbach, M. Taraba, R. Ursin, P. Walther, H. Weier, H. Weinfurter, and A. Zeilinger, “Distributing entanglement and single photons through an intra-city, free-space quantum channel,” *Opt. Express* **13**, 202 (2005).
- [45] C. Z. Peng, T. Yang, X. H. Bao, J. Zhang, X. M. Jin, F. Y. Feng, B. Yang, J. Yang, J. Yin, Q. Zhang, N. Li, B. L. Tian, and J. W. Pan, “Experimental free-space distribution of entangled photon pairs over 13 km: towards satellite-based global quantum communication,” *Phys. Rev. Lett.* **94**, 150501 (2005).
- [46] E. Pazy, E. Biolatti, T. Calarco, I. D’Amico, P. Zanardi, F. Rossi, and P. Zoller, “Spin-based optical quantum computation via Pauli blocking in semiconductor quantum dots,” *Europhys. Lett.* **62**, 175 (2003).
- [47] H. Mabuchi and A. C. Doherty, “Cavity quantum electrodynamics: coherence in context,” *Science* **298**, 1372 (2002).
- [48] A. Imamoglu, D. D. Awschalom, G. Burkard, D. P. DiVincenzo, D. Loss, M. Sherwin, and A. Small, “Quantum information processing using quantum dots spins and cavity QED,” *Phys. Rev. Lett.* **83**, 4204 (1999).